

A Reverberation Lag for the High-Ionization Component of the Broad Line Region in the Narrow-Line Seyfert 1 Mrk 335

C. J. Grier¹, B. M. Peterson^{1,2}, R. W. Pogge^{1,2}, K. D. Denney³, M. C. Bentz⁴,
Paul Martini^{1,2}, S. G. Sergeev⁵, S. Kaspi^{6,7}, Y. Zu¹, C. S. Kochanek^{1,2}, B. J. Shappee¹,
K. Z. Stanek^{1,2}, C. Araya Salvo¹, T. G. Beatty¹, J. C. Bird¹, D. J. Bord⁸, G. A. Borman^{5,9},
X. Che¹⁰, C. Chen¹¹, S. A. Cohen¹¹, M. Dietrich¹, V. T. Doroshenko^{5,9,12}, Yu. S. Efimov^{5,13},
N. Free¹⁴, I. Ginsburg¹¹, C. B. Henderson¹, Keith Horne¹⁵, A. L. King¹⁰, K. Mogren¹,
M. Molina¹, A. M. Mosquera¹, S. V. Nazarov^{5,9}, D. N. Okhmat^{5,9}, O. Pejcha¹, S. Rafter⁷,
J. C. Shields¹⁴, J. Skowron¹, D. M. Szczygiel¹, M. Valluri¹⁰, and J. L. van Saders¹

ABSTRACT

¹Department of Astronomy, The Ohio State University, 140 W 18th Ave, Columbus, OH 43210

²Center for Cosmology & AstroParticle Physics, The Ohio State University, 191 West Woodruff Ave, Columbus, OH 4321, USA

³Dark Cosmology Centre, Niels Bohr Institute, University of Copenhagen, Juliane Maries Vej 30, DK-2100 Copenhagen, Denmark

⁴Department of Physics and Astronomy, Georgia State University, Astronomy Offices, One Park Place South SE, Suite 700, Atlanta, GA 30303, USA

⁵Crimean Astrophysical Observatory, P/O Nauchny Crimea 98409, Ukraine

⁶School of Physics and Astronomy, Raymond and Beverly Sackler Faculty of Exact Sciences, Tel Aviv University, Tel Aviv 69978, Israel

⁷Physics Department, Technion, Haifa 32000, Israel

⁸Department of Natural Sciences, The University of Michigan - Dearborn, 4901 Evergreen Rd, Dearborn, MI 48128

⁹Isaac Newton Institute of Chile, Crimean Branch, Ukraine

¹⁰Department of Astronomy, University of Michigan, 500 Church Street, Ann Arbor, MI 41809

¹¹Department of Physics and Astronomy, Dartmouth College, 6127 Wilder Laboratory, Hanover, NH 03755

¹²Crimean Laboratory of the Sternberg Astronomical Institute, University of Moscow, Russia; P/O Nauchny, 98409 Crimea, Ukraine

¹³Deceased, 2011 Oct 21

¹⁴Department of Physics & Astronomy, Ohio University, Athens, OH 45701

¹⁵SUPA Physics and Astronomy, University of St Andrews, Fife, KY16 9SS Scotland, UK

We present the first results from a detailed analysis of photometric and spectrophotometric data on the narrow-line Seyfert 1 galaxy Mrk 335, collected over a 120-day span in the fall of 2010. From these data we measure the lag in the $\text{He II } \lambda 4686$ broad emission line relative to the optical continuum to be 2.7 ± 0.6 days and the lag in the $\text{H}\beta \lambda 4861$ broad emission line to be 13.9 ± 0.9 days. Combined with the line width, the He II lag yields a black hole mass, $M_{\text{BH}} = (2.6 \pm 0.8) \times 10^7 M_{\odot}$. This measurement is consistent with measurements made using the $\text{H}\beta \lambda 4861$ line, suggesting that the He II emission originates in the same structure as $\text{H}\beta$, but at a much smaller radius. This constitutes the first robust lag measurement for a high-ionization line in a narrow-line Seyfert 1 galaxy and supports a scenario in which the He II emission originates from gas in virial motion rather than outflow.

Subject headings: galaxies: active — galaxies: nuclei — galaxies: Seyfert

1. INTRODUCTION

Narrow-line Seyfert 1 galaxies (NLS1s) are a subset of active galactic nuclei (AGNs) that show narrower broad emission-line components than typical Type 1 AGNs, as well as a number of other distinguishing properties (Osterbrock & Pogge 1985, Goodrich 1989, Boller et al. 1996). Explanations for their unique characteristics include the possibility that they are either low-inclination or high-Eddington rate accreters (or both – see Boroson 2011). Substantial blue enhancements in high ionization lines such as $\text{C IV } \lambda 1549$ and $\text{He II } \lambda 1640$ are apparently typical of, although not restricted to, NLS1 galaxies (e.g., Richards et al. 2002, Sulentic et al. 2000). This may be evidence for material in a disk wind (Richards et al. 2011, Leighly & Moore 2004). If the blue enhancement is due to a wind, the use of high ionization emission lines to measure virial black hole masses (M_{BH}) in these objects may be problematic, as the method relies on the assumption that the emitting gas is in virial motion around the black hole.

To investigate the structure in this region, we turn to reverberation mapping (Blandford & McKee 1982, Peterson 1993). This method has been extensively used to measure the physical size of the broad line region (BLR) in Type 1 AGNs, including NLS1s. Reverberation mapping relies on the correlation between variations of the AGN continuum emission and the subsequent response of the broad emission lines that are seen in Type 1 AGNs. By monitoring AGN spectra over a period of time, one can measure the radius of the emitting gas from the central source by observing a time delay between variations in the continuum and emission line fluxes. Assuming the gas is in virial motion, this radius can be combined with BLR gas

velocity dispersion estimates to obtain a measurement of M_{BH} . To date, this method has been applied to measure BLR radii in nearly 50 AGNs (e.g., Peterson et al. 2004, Denney et al. 2010, Bentz et al. 2010).

If broad high-ionization lines like $\text{He II } \lambda 4686$ are emitted from virialized gas near the black hole, we expect much shorter reverberation time lags for $\text{He II } \lambda 4686$ than for low ionization lines like $\text{H}\beta \lambda 4861$ because both ionization stratification and the line width require this gas to be much closer to the central source. Peterson et al. (2000) investigated the NLS1 NGC 4051 and detected very broad, blue-enhanced $\text{He II } \lambda 4686$ emission in the RMS spectrum. Unfortunately, their time resolution was inadequate to reliably measure a He II lag. Denney et al. (2009) measured an improved $\text{H}\beta$ lag for NGC 4051 using data from their 2007 campaign, but were similarly unable to recover a He II lag. Bentz et al. (2010) report marginal detections of He II lags in two NLS1 galaxies observed in their 2008 observing campaign. These recent studies achieved similar high sampling rates, but the expected He II lags for these targets are too short for a robust detection in these datasets. We have therefore been unable to test whether this emission originates in outflowing gas or is in virial motion.

We included the NLS1 galaxy Mrk 335 in a recent reverberation mapping campaign that will be described in detail elsewhere (Grier et al., in preparation). One goal of this high sampling rate program was to measure the reverberation lag for a high-ionization line, $\text{He II } \lambda 4686$, in this source. Here we present the He II results, having obtained a high enough sampling rate to measure its short time delay, and show that the M_{BH} estimate from the high ionization He II line agrees with those from low ionization lines.

2. OBSERVATIONS

In general, we follow the observational and analysis practices of Denney et al. (2010), which largely follows the analysis described by Peterson et al. (2004). Details on observations and subsequent analysis techniques will be discussed in the accompanying work by Grier et al.

2.1. Spectroscopy

The majority of the spectra were obtained using the 1.3m McGraw-Hill telescope at MDM Observatory. We used the Boller and Chivens CCD spectrograph to obtain 82 spectra over the course of 120 nights from 2010 Aug 31 to Dec 28. We used the 350 mm^{-1} grating to obtain a dispersion of $1.33 \text{ \AA pixel}^{-1}$, with a central wavelength of 5150 \AA and overall

spectral coverage from roughly 4400 Å to 5850 Å. The slit was oriented north-south and set to a width of 5".0 and we used an extraction window of 12".0, which resulted in a spectral resolution of 7.9 Å. Figure 1 shows the mean and root mean square (RMS) spectra of Mrk 335 from the MDM spectra.

We also obtained 7 spectra with the Nasmyth spectrograph and SPEC-10 CCD at the 2.6m Shajn telescope at the Crimean Astrophysical Observatory (CrAO). We used a 3".0 slit at a position angle of 90°. Spectral coverage was from approximately 3900 Å to 6100 Å.

2.2. Photometry

We collected 25 epochs of *V*-band photometry from the 70-cm telescope at CrAO using the AP7p CCD at prime focus, covering a 15'×15' field of view. The flux was measured within an aperture of 15".0. See Sergeev et al. (2005) for more details.

We also obtained 19 epochs of *V*-band photometry at the Wise Observatory of Tel-Aviv University using the Centurion 18-inch telescope with a 3072 × 2048 STL-6303E CCD and a field of view of 75'×50'. For these data, we used the ISIS image subtraction package rather than aperture photometry to measure fluxes (Alard & Lupton 1998; Alard 2000) following the procedure of Shappee & Stanek (2011).

3. LIGHT CURVES AND TIME SERIES ANALYSIS

3.1. Light Curves

The reduced spectra were flux-calibrated assuming that the [O III] λ5007 emission line flux is constant (see Denney et al. 2010 for details on data processing). Emission-line light curves were created for both the MDM and CrAO data sets by fitting linear continua underneath the Hβ and He II lines and integrating the flux above them. Hβ fluxes were measured between 4910–5100 Å in the observed frame, with the continuum interpolation defined by the regions 4895–4910 and 5215–5240 Å. He II λ4686 fluxes were measured from 4660–4895 Å, with the continuum defined from 4550–4575 and 4895–4910 Å. The CrAO light curves were then scaled to the MDM light curve to account for the different amounts of [O III] light that enters the slits due to differences in seeing, slit orientation, and aperture size.

The continuum light curve was created by taking the average 5100 Å continuum flux of the MDM spectra, measured between 5215–5240 Å in the observed frame. This light curve was then scaled and merged with the other continuum and photometric light curves

with corrections for the host galaxy starlight in the different apertures (see Peterson et al. 1995). The final continuum and emission-line light curves are shown in Figure 2. Light curve statistics are given in Table 1.

3.2. Time delay measurements

For comparison with previous results, we used the interpolation method originally described by Gaskell & Sparke (1986) and Gaskell & Peterson (1987) which was later modified by White & Peterson (1994) and Peterson et al. (1998, 2004) to measure the time lag. We cross-correlated the two light curves with one another, calculating the value of the cross correlation coefficient r at each value of time lag. Figure 3 shows the resulting cross correlation functions (CCFs) for the light curves. Uncertainties in lags are calculated using Monte Carlo simulations that employ the methods of Peterson et al. (1998) and refined by Peterson et al. (2004). For each realization, we measure the location of the peak value of the cross correlation coefficient ($\tau_{\text{peak,CCF}}$), and the centroid of the CCF ($\tau_{\text{cent,CCF}}$), calculated using points surrounding the peak. We adopt the mean $\tau_{\text{peak,CCF}}$ and $\tau_{\text{cent,CCF}}$ from the Monte Carlo realizations for our delay measurements and the standard deviation as our formal uncertainties. Before the light curves were cross correlated, we removed the long-term linear upward trend that is clearly visible in all three light curves (see Figure 2). Welsh (1999) discusses the value in this practice of “detrending” the light curves, as the cross correlation function (CCF) tends to latch onto long-term trends unassociated with reverberation, often resulting in incorrect lags. From our cross correlation analysis, we measure $\tau_{\text{cent,CCF}}(\text{H}\beta) = 13.9 \pm 0.9$ days and $\tau_{\text{cent,CCF}}(\text{He II}) = 2.7 \pm 0.6$ days. All lag measurements are listed in Table 2.

Previous reverberation studies have relied on these fairly simple cross correlation methods to measure τ . Recently, however, Zu et al. (2011) discussed an alternative method of measuring reverberation time lags called the Stochastic Process Estimation for AGN Reverberation (SPEAR) and demonstrated its ability to recover accurate time lags. The basic idea is to assume all emission-line light curves are scaled and shifted versions of the continuum light curve. One then fits the light curves using a damped random walk model (e.g. Kelly et al. 2009, Kozłowski et al. 2010, MacLeod et al. 2010) and then aligns them to determine the time lag. Uncertainties in lags are computed using a Markov Chain Monte Carlo method (see Zu et al. 2011). SPEAR is remarkably good at predicting time lags in data sets with relatively large gaps in the sampling. Using SPEAR, we successfully recover time lags for both the $\text{H}\beta$ and He II emission lines. We allowed SPEAR to automatically remove the linear trend and include any resulting uncertainties in the overall lag uncertainties. We measure $\tau_{\text{SPEAR}}(\text{H}\beta) = 14.0 \pm 0.3$ days and $\tau_{\text{SPEAR}}(\text{He II}) = 1.6^{+0.7}_{-0.5}$ days, also reported in

Table 2. We see good agreement with the CCF results from the $H\beta$ emission line, and while there is a small difference between SPEAR and CCF lags for the He II line, they are still statistically consistent with one another. We suspect this small difference is due to the gap in data that is very close to the peak in the He II light curve. We adopt the CCF values for our mass calculations to allow comparison with previous reverberation efforts.

3.3. Line width measurement and M_{BH} calculations

Assuming that the motion of the $H\beta$ -emitting gas is dominated by gravity, the relation between M_{BH} , line width, and time delay is

$$M_{\text{BH}} = \frac{f c \tau \Delta V^2}{G}, \quad (1)$$

where τ is the measured emission-line time delay, ΔV is the velocity dispersion of the BLR, and f is a dimensionless factor that accounts for the structure within the BLR. The BLR velocity dispersion can be estimated using the line width of the measured broad emission line in question. This width is usually characterized by either the FWHM or the line dispersion, σ_{line} . We use σ_{line} because there is evidence that it produces less biased M_{BH} measurements (Peterson 2011). We measure the line width in the RMS spectrum, which eliminates contributions from the contaminating narrow components. We adopt an average value of $\langle f \rangle = 5.5$ based on the assumption that AGNs follow the same $M_{\text{BH}} - \sigma_*$ relationship as quiescent galaxies (Onken et al. 2004). This is consistent with Woo et al. (2010) and allows easy comparison with previous results, but is about a factor of two larger than the value of $\langle f \rangle$ computed by Graham et al. (2011).

To determine the best value of σ_{line} , we use Monte Carlo simulations following Peterson et al. (2004). The resulting line widths are given in Table 2. Using our measured values of $\tau_{\text{cent,CCF}}$ for the average time lag and σ_{line} from the RMS spectrum as ΔV , we compute M_{BH} using both the $H\beta$ and He II emission lines. We measure $M_{\text{BH}} = (2.7 \pm 0.3) \times 10^7 M_{\odot}$ using the $H\beta$ emission line and $M_{\text{BH}} = (2.6 \pm 0.6) \times 10^7 M_{\odot}$ using He II.

4. DISCUSSION

As discussed above, several studies involving NLS1 galaxies have found indications of outflows in high-ionization lines in the form of enhanced flux on the blue side of the emission lines. Inspection of Mrk 335 spectra from the *HST* archive shows this enhanced blueward flux is present in the C IV $\lambda 1549$ line as well, but the He II $\lambda 1640$ line is blended with C IV, so

we cannot see if it too exhibits this blue enhancement. In fact, the shape of the He II $\lambda 4686$ emission line in the RMS spectrum of Mrk 335 (Figure 1) shows red and blue shoulders that could be a signature of disk structure. To search for possible outflow signatures in the He II $\lambda 4686$ emission line, we divided it into red and blue components and integrated each component separately, creating two He II light curves. We then cross-correlated the red and blue light curves with one another to see if there is any time delay between the two components. Cross correlation analysis yields a centroid lag $\tau_{\text{cent}} = 0.4 \pm 0.8$ days. This is consistent with zero and thus presents no evidence for bulk outflows in the He II $\lambda 4686$ emission of Mrk 335. The consistency of the M_{BH} measurements made using the He II lines with those from H β are also suggestive of virial motion rather than outflowing gas.

Previous reverberation measurements of Mrk 335 were made by Kassebaum et al. (1997) and Peterson et al. (1998) and subsequently reanalyzed by Peterson et al. (2004) and Zu et al. (2011). Zu et al. (2011) report a time delay of $15.3^{+3.6}_{-2.2}$ days and $\sigma_{\text{line}} \sim 920 \text{ km s}^{-1}$ for H β , but were unable to make a robust He II measurement, as their average time sampling was on the order of 10 days. Peterson et al. (2004) measure $M_{\text{BH}} = (1.4 \pm 0.4) \times 10^7 M_{\odot}$ from the H β emission line. Our M_{BH} measurements deviate from theirs by almost a factor of two. We suspect the difference in M_{BH} is due to the difference in the line width measurements between the two campaigns. The uncertainties in line width measurements and in the f factor are the main sources of uncertainties in reverberation M_{BH} measurements – when the light curves are well-sampled, the lag measurements themselves have been shown to be remarkably robust (e.g. Watson et al. 2011). Peterson et al. (2004) (Table 6) find that the virial products computed for an object using data from different epochs often differ from one another by as much as a factor of two (e.g. NGC 5548) and that the typical fractional error in the virial products is about 33%. Given our uncertainties in the f factor and the limitations in trying to accurately describe the BLR velocity field with a single line-width characterization, we probably cannot actually do better than about a factor of two or three in individual M_{BH} measurements.

Ground-based reverberation campaigns in the past have been limited to objects with H β time lags that are expected to be less than a month or two due to both the finite length of the campaigns (which typically last 50–100 days) and the fact that most objects are only observable from the ground for only about half of the year. Measurement of longer time lags would require extended campaigns, which are difficult to schedule. If, as our evidence suggests, the He II emission line is in virial motion around the black hole, we can use this emission line to measure M_{BH} in objects at higher redshifts, as expected He II lags in many of these high-luminosity objects are short enough to measure in one observing season.

5. SUMMARY

We have presented the first robust He II $\lambda 4686$ reverberation lag measurement in a NLS1 galaxy. We also measure the H β time lag in this galaxy and compute M_{BH} using both emission lines. The M_{BH} measurements from He II and H β are consistent with one another, suggesting that the gas producing the He II emission resides in the same structure as that producing H β emission. While other high-ionization lines such as C IV show evidence for outflows, we do not see this in He II, possibly because the He II-emitting gas does not arise cospatially with gas producing C IV emission. This has practical implications for future reverberation efforts, as the He II emission may allow us to more efficiently measure M_{BH} in objects at high redshift.

We gratefully acknowledge the support of the National Science Foundation through grant AST-1008882. BJS, CBH, and JLV are supported by NSF Fellowships. CSK and DMS acknowledge the support of NSF grant AST-1004756. AMM acknowledges the support of Generalitat Valenciana, grant APOSTD/2010/030. SK is supported at the Technion by the Kitzman Fellowship. SK and SR are supported by a grant from the Israel-Niedersachsen collaboration program. SR is also supported at Technion by the Lady Davis Fellowship. SGS acknowledges the support to CrAO in the frame of the 'CosmoMicroPhysics' Target Scientific Research Complex Programme of the National Academy of Sciences of Ukraine (2007-2012). VTD acknowledges the support of the Russian Foundation of Research (RFBR, project no. 09-02-01136a). The CrAO CCD cameras were purchased through the US Civilian Research and Development for Independent States of the Former Soviet Union (CRDF) awards UP1-2116 and UP1-2549-CR-03. This research has made use of the NASA/IPAC Extragalactic Database (NED) which is operated by the Jet Propulsion Laboratory, California Institute of Technology, under contract with the National Aeronautics and Space Administration.

REFERENCES

- Alard, C. 2000, A&AS, 144, 363
- Alard, C., & Lupton, R. H. 1998, ApJ, 503, 325
- Bentz, M. C., et al. 2010, ApJ, 716, 993
- Blandford, R. D., & McKee, C. F. 1982, ApJ, 255, 419
- Boller, T., Brandt, W. N., & Fink, H. 1996, A&A, 305, 53

- Boroson, T. A. 2011, in *Narrow-Line Seyfert 1 Galaxies and their Place in the Universe*
- Denney, K. D., et al. 2009, *ApJ*, 702, 1353
- . 2010, *ApJ*, 721, 715
- Gaskell, C. M., & Peterson, B. M. 1987, *ApJS*, 65, 1
- Gaskell, C. M., & Sparke, L. S. 1986, *ApJ*, 305, 175
- Goodrich, R. W. 1989, *ApJ*, 342, 224
- Graham, A. W., Onken, C. A., Athanassoula, E., & Combes, F. 2011, *MNRAS*, 412, 2211
- Kassebaum, T. M., Peterson, B. M., Wanders, I., Pogge, R. W., Bertram, R., & Wagner, R. M. 1997, *ApJ*, 475, 106
- Kelly, B. C., Bechtold, J., & Siemiginowska, A. 2009, *ApJ*, 698, 895
- Kozłowski, S., et al. 2010, *ApJ*, 708, 927
- Leighly, K. M., & Moore, J. R. 2004, *ApJ*, 611, 107
- MacLeod, C. L., et al. 2010, *ApJ*, 721, 1014
- Onken, C. A., Ferrarese, L., Merritt, D., Peterson, B. M., Pogge, R. W., Vestergaard, M., & Wandel, A. 2004, *ApJ*, 615, 645
- Osterbrock, D. E., & Pogge, R. W. 1985, *ApJ*, 297, 166
- Peterson, B. M. 1993, *PASP*, 105, 247
- Peterson, B. M. 2011, in *Narrow-Line Seyfert 1 Galaxies and their Place in the Universe*
- Peterson, B. M., Pogge, R. W., Wanders, I., Smith, S. M., & Romanishin, W. 1995, *PASP*, 107, 579
- Peterson, B. M., Wanders, I., Bertram, R., Hunley, J. F., Pogge, R. W., & Wagner, R. M. 1998, *ApJ*, 501, 82
- Peterson, B. M., et al. 2000, *ApJ*, 542, 161
- . 2004, *ApJ*, 613, 682
- Richards, G. T., Vanden Berk, D. E., Reichard, T. A., Hall, P. B., Schneider, D. P., SubbaRao, M., Thakar, A. R., & York, D. G. 2002, *AJ*, 124, 1

- Richards, G. T., et al. 2011, *AJ*, 141, 167
- Sergeev, S. G., Doroshenko, V. T., Golubinskiy, Y. V., Merkulova, N. I., & Sergeeva, E. A. 2005, *ApJ*, 622, 129
- Shappee, B. J., & Stanek, K. Z. 2011, *ApJ*, 733, 124
- Sulentic, J. W., Zwitter, T., Marziani, P., & Dultzin-Hacyan, D. 2000, *ApJ*, 536, L5
- Watson, D., Denney, K. D., Vestergaard, M., & Davis, T. M. 2011, *ApJ*, 740, L49
- Welsh, W. F. 1999, *PASP*, 111, 1347
- White, R. J., & Peterson, B. M. 1994, *PASP*, 106, 879
- Woo, J.-H., et al. 2010, *ApJ*, 716, 269
- Zu, Y., Kochanek, C. S., & Peterson, B. M. 2011, *ApJ*, 735, 80

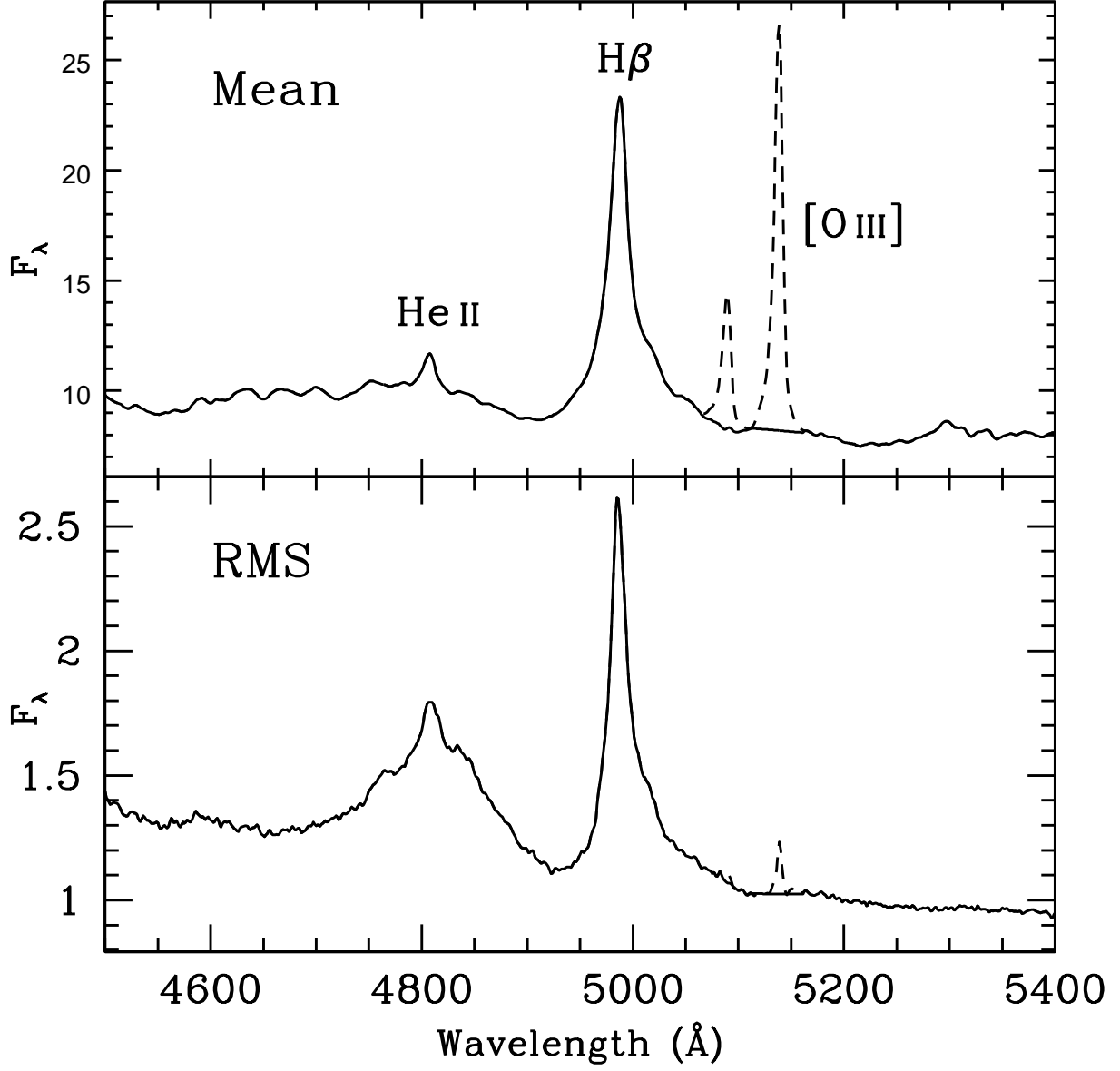


Fig. 1.— The flux-calibrated mean (top) and RMS (bottom) spectra of Mrk335 in the observed frame ($z = 0.02579$). The flux density is in units of $10^{-15} \text{ erg s}^{-1} \text{ cm}^{-2} \text{ \AA}^{-1}$. The dashed lines show the spectra before the [O III] narrow emission lines were removed; the solid line shows the spectra after the subtraction.

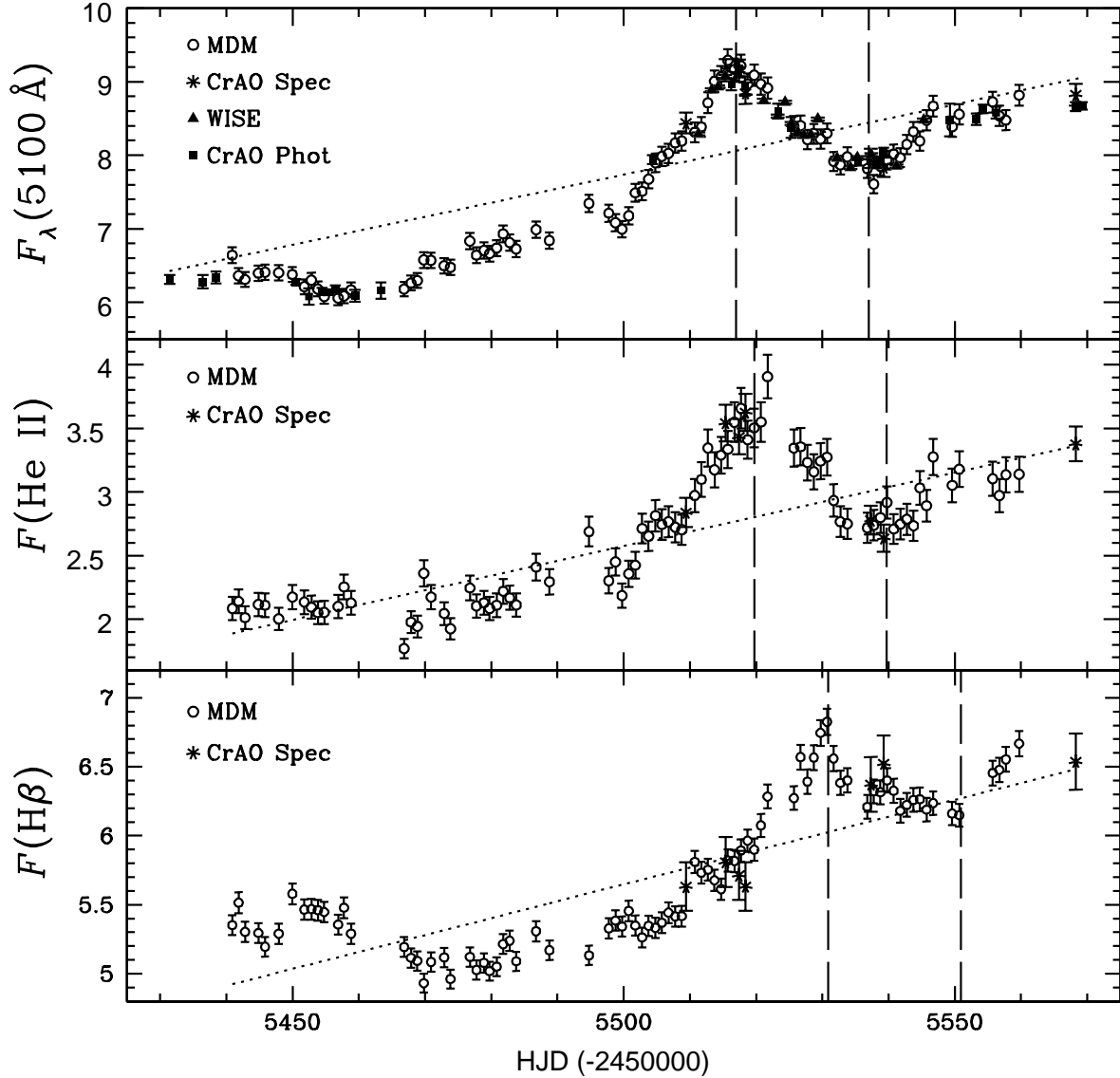


Fig. 2.— Complete light curves for Mrk 335 from our observing campaign. The top panel shows the 5100Å flux in units of $10^{-15} \text{ erg s}^{-1} \text{ cm}^{-2} \text{ Å}^{-1}$, the middle panel shows the flux in the He II $\lambda 4686$ region in units of $10^{-13} \text{ erg s}^{-1} \text{ cm}^{-2}$, and the bottom panel shows the integrated H β $\lambda 4861$ flux, also in units of $10^{-13} \text{ erg s}^{-1} \text{ cm}^{-2}$. Open circles denote observations from MDM Observatory and asterisks represent spectra taken at CrAO. Closed squares show the photometric observations from CrAO, and closed triangles represent photometric observations from WISE Observatory. Vertical dashed lines have been placed at two obvious features in the continuum to aid the eye. The vertical lines have been shifted by the measured He II and H β lag values (2.7 days and 13.9 days, respectively) to aid the eye in identifying the correct lag values for each emission line. Dotted lines show the trends that were subtracted before performing the cross correlation analysis.

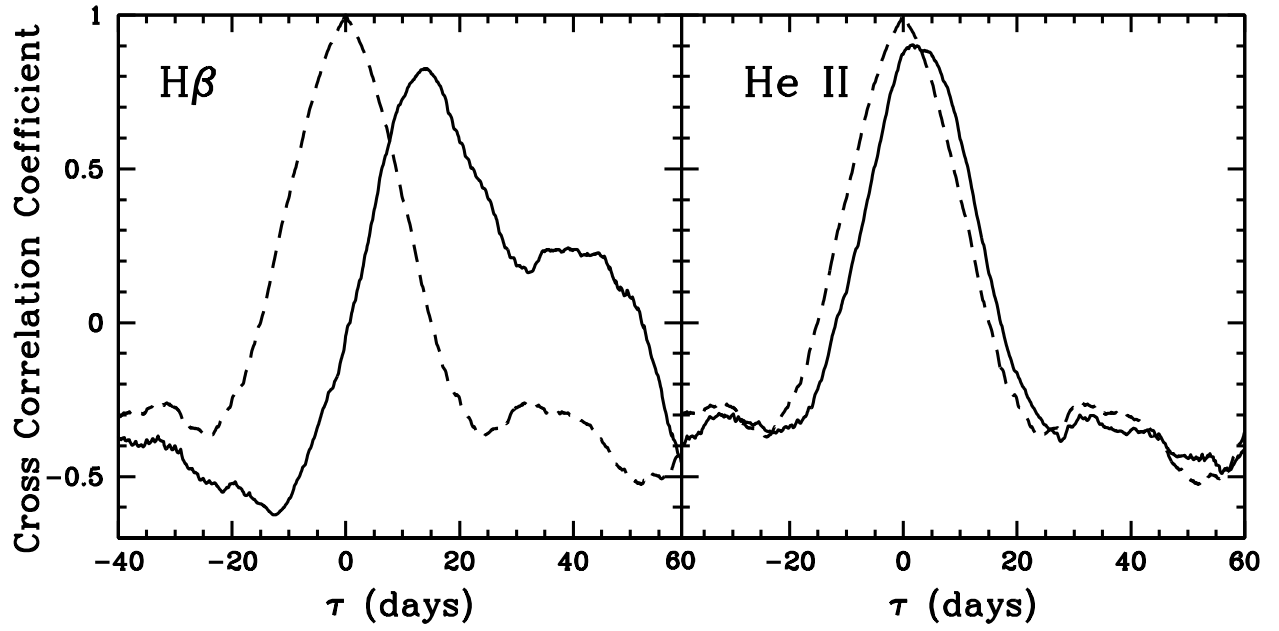


Fig. 3.— CCFs for the light curves. Dashed lines represent the autocorrelation function (ACF) of the continuum light curve, and solid lines show the CCFs for the emission lines.

Table 1. Light Curve Statistics

Time Series (1)	N (2)	Sampling Interval (days)		Mean Flux (5)	Mean Fractional Error		
		$\langle T \rangle$ (3)	T_{median} (4)		(6)	F_{var} (7)	R_{max} (8)
5100 Å	133	1.0	0.95	7.57 ± 1.01	0.013	0.129	1.53 ± 0.04
He II $\lambda 4686$	89	1.5	1.00	7.65 ± 1.00	0.016	0.130	1.55 ± 0.04
H β $\lambda 4861$	89	1.5	1.00	5.74 ± 0.53	0.015	0.091	1.38 ± 0.03

*Column (1) lists the spectral feature, and column (2) gives the number of points in the individual light curves. Columns (3) and (4) list the average and median time spacing between observations, respectively. Column (5) gives the mean flux of the feature in the observed frame, and column (6) shows the mean fractional error that is computed based on observations that are closely spaced in time. Column (7) gives the excess variance, defined by

$$F_{\text{var}} = \frac{\sqrt{\sigma^2 - \delta^2}}{\langle f \rangle} \quad (2)$$

where σ^2 is the flux variance of the observations, δ^2 is the mean square uncertainty, and $\langle f \rangle$ is the mean observed flux. Column (8) is the ratio of the maximum to minimum flux in each light curve.

*Continuum and emission-line fluxes are given in $10^{-15} \text{ erg s}^{-1} \text{ cm}^{-2} \text{ Å}^{-1}$ and $10^{-13} \text{ erg s}^{-1} \text{ cm}^{-2}$, respectively.

Table 2. $H\beta$ and $\text{He II } \lambda 4686$ Time Series Results

Parameter (1)	$H\beta$ (2)	He II (3)
$\tau_{\text{cent,CCF}}^{\text{a}}$	13.9 ± 0.9 days	2.7 ± 0.6 days
$\tau_{\text{peak,CCF}}^{\text{b}}$	13.8 ± 0.8 days	2.1 ± 1.2 days
τ_{SPEAR}	14.0 ± 0.3 days	$1.6^{+0.7}_{-0.5}$ days
σ_{line} (mean)	1641 ± 12 km s $^{-1}$	3465 ± 26 km s $^{-1}$
FWHM (mean)	1363 ± 15 km s $^{-1}$	3191 ± 571 km s $^{-1}$
σ_{line} (RMS)	1336 ± 51 km s $^{-1}$	3001 ± 277 km s $^{-1}$
FWHM (RMS)	1149 ± 38 km s $^{-1}$	7380 ± 1275 km s $^{-1}$
M_{BH}	$(2.7 \pm 0.3) \times 10^7 M_{\odot}$	$(2.6 \pm 0.8) \times 10^7 M_{\odot}$

*All values are given in the rest frame of the object.